McMaster University | ENGINEERING

This paper is the final draft post-refereeing of the following article:

Kovacs M, Wiebe L. 2019. Controlled rocking heavy timber walls for buildings in regions of moderate seismicity: design procedure and numerical collapse assessment. *Journal of Earthquake Engineering*, 23(5): 750-770.

The DOI is [10.1080/13632469.2017.1326421](https://doi.org/10.1080/13632469.2017.1326421).

This version is posted in accordance with the copyright restrictions of Taylor & Francis, as described at:

http://sherpa.ac.uk/romeo/issn/1363-2469/

BRIGHTER WORLD

TITLE: Controlled Rocking CLT Walls for Buildings in Regions of Moderate Seismicity: Design Procedure and Numerical Collapse Assessment

ABSTRACT: Controlled rocking heavy timber walls are designed to rock on their foundation in response to seismic loads. For regions of moderate seismicity, it is proposed that this rocking behaviour can be adequately controlled by using only post-tensioning, even with a large force-reduction factor and no supplemental energy dissipation. This article presents a force-based design procedure for controlled rocking heavy timber walls made of cross-laminated timber (CLT), without supplemental energy dissipation, including a simple theory-based method for estimating higher mode effects. Based on nonlinear time-history analyses of three prototype walls, fragility analyses demonstrate that the design procedure can limit the probability of collapse to less than 10% during a maximum considered earthquake in a region of moderate seismicity.

Published Article Available from Taylor & Francis:

http://dx.doi.org/10.1080/13632469.2017.1326421

1. Introduction

High-performance structural systems are increasingly being adopted to mitigate seismic risk in regions with high seismic hazard. However, even regions with more moderate seismic hazard still face significant seismic risks as urban centres densify to accommodate growing populations [Blaikie et al. 2003]. In these regions, a low perception of seismic risk can result in opposition to high-performance structural alternatives that are considered complex and expensive [Fischer III et al. 1996]. To overcome this challenge, high-performance solutions can be combined with other features desired by stakeholders. For example, Natural Resources Canada [2013] has identified Cross-Laminated Timber (CLT) as an environmentally and economically advantageous construction material for both Canada and the United States. Some key advantages of CLT are its low-carbon footprint, the use of low-grade timber, and the potential for more efficient construction using CLT as the primary wall, floor, and roof elements [Moses and Gagnon 2010; Structural Timber Association 2014]. Considering also the increasing market supply of CLT [Pei et al. 2016], there is an opportunity to adapt high-performance CLT-based structural alternatives to regions of low-to-moderate seismicity.

One potential high-performance solution is the controlled rocking heavy timber wall. Controlled rocking heavy timber walls were first developed and implemented in New Zealand, primarily using Laminated Veneer Lumber (LVL), to reduce seismic loads and mitigate structural damage due to large seismic events [Palermo et al. 2005]. The controlled rocking heavy timber wall is designed to rock on its foundation in response to seismic loads, so as to limit seismic forces imposed on the structure. The rocking behaviour is controlled by post-tensioning and supplemental energy dissipation elements. Most controlled rocking heavy timber wall studies have focused on LVL products, as opposed to CLT. Compared to LVL, the controlled rocking CLT wall panel is expected to be less stiff and to have a softer rocking interface at the foundation due to the material properties of CLT [Structural Timber Association 2014]. This will affect the global performance of the system and must be considered in addition to several other controlled rocking wall design and performance issues outlined herein.

First, timber products are susceptible to short-term dimensional changes due to moisture and temperature variations, especially in unidirectional timber materials like LVL and glulam. Dimensional changes affect the controlled rocking wall by modifying the post-tensioning forces [Davies and Fragiacomo, 2011; Morris et al., 2012]. These dimensional variations can be addressed by using more stable engineered timber products like LVL produced with alternating laminate directions, or using cross-laminated timber. In addition, when timber products are post-tensioned, there is also increased potential for long-term creep effects [Davies and Fragiacomo 2011; Yeoh et al. 2012]. Long-term post-tensioning challenges due to creep can be overcome using design details that spread the post-tensioning forces over a larger area [Sarti 2015]. Furthermore, recent research has suggested that relatively large force reduction factors could be used in the force-based design of controlled rocking systems, while still controlling the peak displacements to within acceptable limits [Zhang 2015]. This suggests that the post-tensioning demand could be reduced by designing with a larger force reduction factor, but this has not yet been explored for controlled rocking heavy timber walls.

Another concern with the performance of controlled rocking heavy timber walls is the potential for damage at the connections to supplemental energy dissipation devices [Sarti et al. 2015]. Researchers are developing inexpensive, replaceable supplemental energy dissipation elements to mitigate connection damage [Iqbal et al. 2012; Sarti et al. 2015]. However, omitting supplemental energy dissipation altogether could be considered to avoid this damage if doing so did not lead to undesirable system-level performance, but this possibility has not yet been explored. Moreover, regardless of the amount of supplemental energy dissipation that is provided, the forces above the base of a controlled rocking heavy timber wall are likely to be significantly influenced by higher mode effects, but current methods for estimating the higher mode response require calibration to experimental data and have demonstrated inconsistent performance [Sarti 2015].

This article seeks to address how controlled rocking CLT walls could be applied in regions with moderate seismic hazard. First, the base connection and higher mode response of a controlled rocking CLT wall without supplemental energy dissipation is described. This provides background for a force-based design and analysis procedure that is presented for a controlled rocking CLT wall without supplemental energy dissipation. Supplemental energy dissipation is omitted to minimise design and construction cost and complexity, and this paper examines whether this can be done while still controlling the peak displacement response. Accordingly, the force-based procedure includes a method to estimate the peak displacement of the controlled rocking CLT wall, which also allows the designer to minimise the post-tensioning requirements by selecting a relatively large force-reduction factor. A higher mode estimation process is also described based on a similar procedure for controlled rocking steel braced frames. Next, three-, six-, and nine-storey controlled rocking CLT wall prototypes are designed for the moderate seismic hazard of Montreal, Canada, and each prototype is modelled with OpenSees and subjected to incremental dynamic analysis. The response of each wall to a 2% in 50-year seismic hazard is investigated, and fragility curves are also developed to assess the probability of collapse or of exceeding the shear or bending moment capacity of the CLT panels.

2. Controlled Rocking CLT Wall Mechanics

2.1 Quasi-Static Response

A controlled rocking CLT wall without supplemental energy dissipation elements behaves as shown in Figure 1 (a-d), and the base connection moment-roof drift response (M_{base}-θ_{roof}) is shown in Figure 1 (e). Low seismic or wind loads cause elastic shear and bending drifts (θ_s and θ_f; cumulatively, θ_{el}) as shown in Figure 1 (a,b). When the seismic loads are large enough to overcome the post-tensioning (PT) and cause decompression in the base, the wall enters the nonlinear elastic range described by Figure 1 (c), causing a base connection rotation (θ_{con}). This causes elongation of the PT, which provide a positive stiffness to the M_{base}-θ_{roof} response. When the load is removed, the base connection rotation (θ_{con}) reduces until the system returns to its original position (Figure 1 (d)). The system would repeat this response in the opposite direction. Figure 1 (e) shows two different load paths: the dotted line is an elastic load path, reflecting the M_{base} demand on a system that is designed to respond elastically without rocking (M_{el}). Alternatively, the non-linear path reflects the controlled rocking response in which the system begins to rock when M_{base} reaches a design moment (M_{con}).

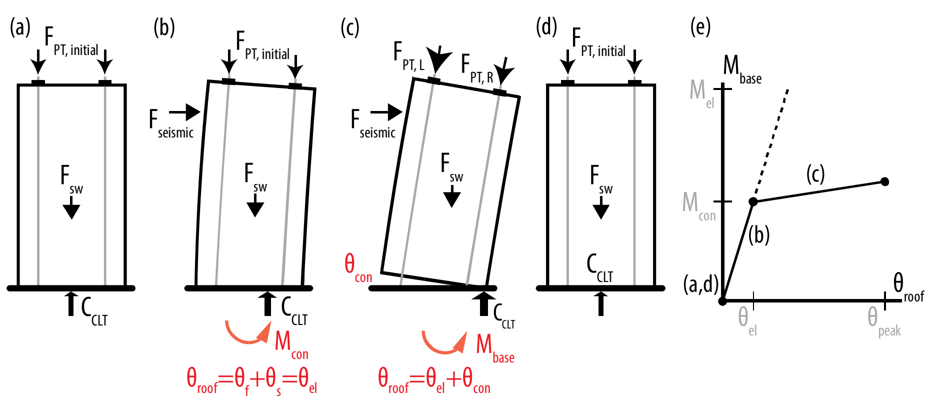

Figure 1 - General controlled rocking CLT system response

2.2 Rocking & Base Connection Mechanics of Controlled Rocking CLT Walls

Earthquake loading imposes drifts, θ_f, θ_s, and θ_{con}, on the controlled rocking CLT wall, as shown in Figure 2 (a). The contribution that is caused by base uplift is associated with a compression interface between the timber and foundation, as shown in Figure 2 (b). The uplift also elongates the PT tendons, creating overturning moment resistance, M_{base}, that returns the wall towards its original position. The relationship between M_{base} and θ_{con} is quantified in this paper using the Winkler Spring Analogy [Newcombe 2011, 2015] which represents the base connection interface as a series of springs with axial stiffness, $E_{timber}A/L_{eff}$, where L_{eff} is defined in Eqn. (1) as a function of the wall length (l_w) and neutral axis depth (c) [Newcombe 2011, 2015].

$$L_{eff} = 120\left(\frac{l_w}{c} - 1\right) \tag{1}$$

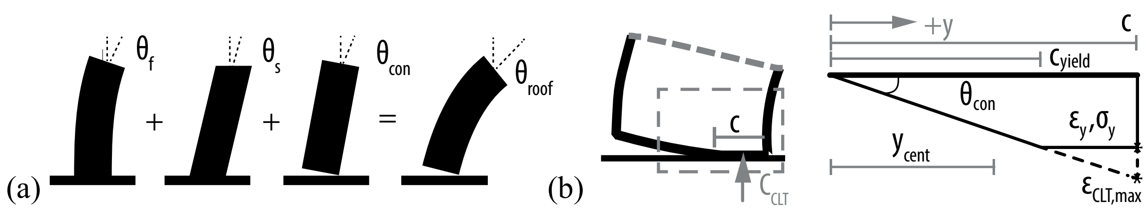

Figure 2 - (a) Flexure, shear, and rigid body rotation of controlled rocking CLT; (b) Effect on rocking toe

When analysing the base connection response, the relationship between L_{eff} and c can be recalculated for individual θ_{roof} responses of interest (e.g. at several points in a quasi-static pushover response). The c-L_{eff} relationship is also used for numerical modelling; however, it is computationally expensive to solve for c at every θ_{con} during time history analysis. Therefore, for numerical modelling, a constant L_{eff} term is determined based on c when θ_{roof} reaches its maximum value (typically assumed to be 2-2.5%) [Newcombe 2015].

The following analysis process uses the Winkler spring analogy to determine the timber compression (C_{CLT}) contribution to M_{base}, in calculating the base connection and controlled rocking wall response at selected θ_{con}. The process is based on research by Newcombe [2011, 2015] and Sarti [2015]. Further details of the process for the adapted controlled rocking CLT wall are presented by Kovacs [2016].

In order to determine the controlled rocking CLT wall response at a selected θ_{con}, a corresponding c is assumed, and L_{eff} is calculated from Eq. (1). Next, the rocking toe interface is evaluated using the strain profile shown in Figure 2 (b) ($\varepsilon_{CLT}=\theta_{con}c/L_{eff}$). The strain profile is converted to a stress profile considering a bilinear material relationship: σ_y and c_{yield} are the yield stress and corresponding depth from the neutral axis to the timber yield point, respectively. C_{CLT} and the centroid of the compression toe stress block (y_{cent}) are determined by integration and summation of moments, respectively.

The PT forces (PT_1, PT_2) are calculated next: the initial PT force ($T_{PT,init}$) is modified by the elongation due to rocking, as shown in Figure 3. The vertical and horizontal components of the PT force are determined by considering the system geometry and PT material properties at the selected θ_{con}.

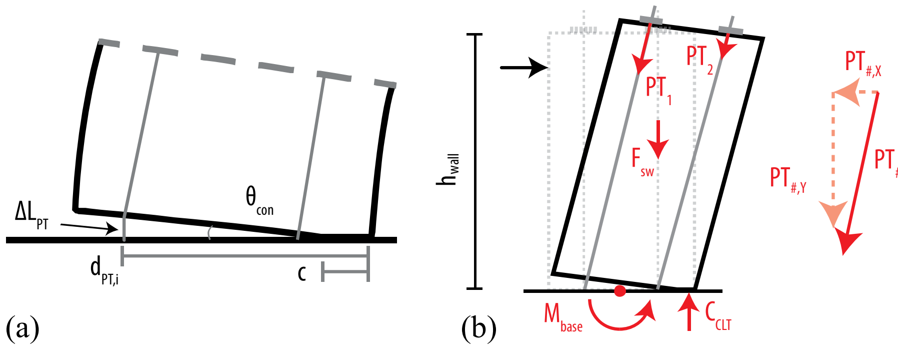

Figure 3 - (a) Elongating PT due to rocking; (b) Contributions to M_{base}

Next, force equilibrium is checked at the base connection interface, considering C_{CLT}, PT_1 and PT_2, and wall self-weight (F_{sw}). If equilibrium is not satisfied, it is necessary to iterate the analysis with a new c. If equilibrium is satisfied, then M_{base} is determined from the components in Figure 3 (b). In a tall controlled rocking CLT wall, the horizontal PT force contribution at the roof can become significant as θ_{con} increases, so both the horizontal and vertical components of the PT force are calculated. The base shear (V_b) is determined by dividing M_{base} by the effective height of the structure ($H_{eff}=\sum(m_i h_i^2)/\sum(m_i h_i)$, where m_i and h_i are the masses of storey i, and height of storey i, respectively).

Finally, θ_{roof} is determined by considering the sum of bending and shear drifts (θ_f and θ_s respectively) and adding θ_{con}. θ_f and θ_s are determined using conventional structural mechanics, and Sarti [2015] developed a simplified equation for θ_f and θ_s:

$$\theta_f + \theta_s = \theta_{el} = M_{base}\left(\frac{H}{6E_b I}k_b + \frac{k_s}{GA_v H}\right)$$
$$\text{where } k_b = \frac{\sum_{j=1}^{n} j^3\left(3-\frac{j}{n}\right)}{\sum_{j=1}^{n} j^2} \quad \text{and} \quad k_s = \frac{1}{n} \tag{2}$$

In Eqn. (2), j refers to storey j, n is the number of storeys, H is the storey height, E_b is the bending modulus of the timber panel, I is the moment of inertia about the bending axis, and G and A_v are the shear modulus and area, respectively. A widely-spaced PT configuration creates a concentrated moment at the top of the wall due to the difference in PT forces imposed when large drifts are considered. This moment imposes bending in the direction opposite to the rocking motion, and should be considered when calculating the total flexural drift [Kovacs 2016].

2.3 Higher Mode Response

The general controlled rocking CLT wall behaviour described in Sections 2.1 and 2.2 is based on the first-mode response, which is assumed to dominate the roof displacement. However, higher mode vibrations can increase bending moment and shear force demands over the height of the wall; these must be considered for capacity design [Sarti 2015], as shown in findings with controlled rocking LVL wall research [Newcombe 2011]. With CLT panels, the effect of higher mode vibrations is potentially even more significant because of CLT's lower stiffness and strength compared to LVL, affecting the wall's dynamic properties and capacity to resist the associated demands. Sample properties and associated effects are shown in Table 1. Furthermore, ground motions with relatively high frequency content, as expected in regions where earthquakes of smaller magnitude dominate the seismic hazard [Tsinker 1997], are expected to result in more significant higher mode effects. Therefore, a higher mode estimation procedure, referred to as the cantilever beam analogy, is presented as part of the capacity design process in Section 3.2.

Table 1 - Comparison of CLT and LVL properties, and resulting behavioural effects

Property Parameter	**Difference from LVL [1]**	**Value [2] (gross section)**	**Expected Effect**
Comp. Strength, f_c	60-70% Lower	13 MPa	Toe crushing more likely
Bending Strength, $f_{b,eff}$	50-60% Lower	19 MPa	Bending failure more likely
Elastic Modulus, E	40-50% Lower	7,900 MPa	Increased elastic drift Increased higher mode demands
Shear Modulus, G	20-25% Lower	520 MPa	Increased elastic drift Increased higher mode demands

[1] Comparing values from [Flaig and Blass 2013] with [Sarti 2015]
[2] From KLH UK [2015], Newcombe [2011]; Sarti [2015]

3. Design Methodology

Following Wiebe & Christopoulos [2015a], the proposed design methodology has two main parts. The base connection design procedure is presented first, relying on the base connection mechanics presented in Section 2.2. The capacity design process is presented second, comparing higher mode demand estimates to bending and shear capacity estimates.

3.1 Base Connection Design

An initial estimate of the natural period (T_1) is required for the first design iteration, after which the period of the structure as designed can be used.

Next, a force reduction factor (R) is specified. This value may be iterated to control the estimated drift demand and to avoid unnecessarily reducing the seismic base overturning moment to be less than the wind base overturning moment. After the seismic and wind demands are calculated, the minimum quantity of walls to resist the governing overturning moment (M_{con}) can be determined by approximating an initial PT force and l_w dimension and calculating the resisting moment about a rocking toe. CLT panels and PT bars should be selected to minimise long term timber damage and to avoid PT yielding. Further considerations for the selection of a CLT panel and PT bar are provided by Kovacs [2016].

Given a preliminary selection of the number of walls, and the CLT panel and PT bar properties and configuration, the required initial PT force ($T_{PT,init}$) is calculated. The mechanics of Section 2.2 can be used for this calculation, but a simplification is shown in Figure 4 based on the assumption that the rocking toe compression interface will remain elastic before rocking, and that the cumulative PT force will be unchanged from $T_{PT,init}$, as shown by Kovacs [2016]. Sarti [2015] assumed the neutral axis location (c) to be at 30% of l_w, but Kovacs [2016] showed that considering the neutral axis to be at the first PT element (c=d_{PT1}) was both simple and sufficiently accurate if the PT elements are spaced at 25% and 75% of l_w. The required PT force to resist M_{con} is determined by Eqn. (3), where the PT elements are assumed to be located symmetrically about the centre of the wall (i.e. d_{PT2}=l_w-d_{PT1}).

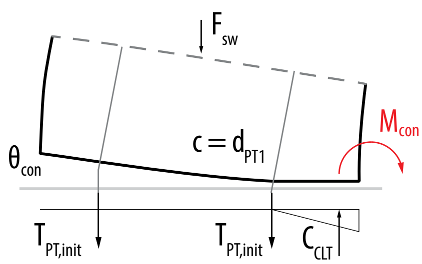

Figure 4 - Free body diagram of base connection for design

$$T_{PT,init} = \frac{M_{con} - F_{sw}\left(\frac{l_w}{2} - \frac{d_{PT1}}{3}\right)}{l_w - \frac{2d_{PT1}}{3}} \tag{3}$$

An estimate of the peak roof drift (θ_{peak}) is required to check against the performance requirements (e.g. the Canadian building code specifies a maximum of 2.5% roof drift in a 2%/50-year earthquake for buildings of normal importance [NRCC 2010]). An empirical correction factor (C_R) is used to estimate θ_{peak}, based on research by Zhang [2015]. To estimate θ_{peak}, the elastic roof drift (θ_{el}) is determined using Eqn. (2), where M_{base} is taken as M_{con}. Next, the result is multiplied by R and C_R, where C_R was calibrated by Zhang [2015] for self-centering SDOF systems using west coast-type records:

$$C_R = \frac{\theta_{peak}}{\theta_{el}} = (R-1)^{0.63}\frac{0.292 + 0.477(1-\beta)^{1.697}}{T_1^{1.567}} + 1 \tag{4}$$

Eqn. (4) was calibrated for systems with a minimum amount of energy dissipation, β (i.e. β≥0.2), and was generally conservative when no energy dissipation was included (i.e. β=0) [Zhang 2015]. If θ_{peak} is excessive, it can be reduced by changing the wall panel dimensions or timber material, or by reducing the force reduction factor.

3.2 Capacity Design: Higher Mode Estimation

A cantilever beam analogy was presented by Wiebe and Christopoulos [2015b; c] to predict the higher mode response of controlled rocking steel braced frames. In this method, the peak shear and moment response contributions ($V_{i,max}$ and $M_{i,max}$, respectively) are calculated from the first, second, and third modes of vibration of a cantilever shear beam using Eqns. (5)-(10) [Wiebe and Christopoulos 2015b], where M_{con} is the design base connection moment, h_j is the height of storey j above the base, h_w is the total wall height, and $S_a(T_i)$ is the spectral acceleration at the period for mode i.

$$V_{1\max} = \frac{3}{2}\left(\frac{\Omega M_{con}}{h_w}\right)\left[1 - \frac{h_j}{h_w}^2\right] \tag{5}$$

$$V_{2\max} = 0.1265 S_a\left(T_2\right)\frac{W_{trib}}{g}\left|\cos\frac{4.49h_j}{h_w} + 0.217\right| \tag{6}$$

$$V_{3\max} = 0.0297 S_a\left(T_3\right)\frac{W_{trib}}{g}\left|\cos\frac{7.73h_j}{h_w} - 0.1283\right| \tag{7}$$

$$M_{1\max} = \Omega M_{con}\left[1 - (3/2)\frac{h_j}{h_w} + (1/2)\frac{h_j}{h_w}^3\right] \tag{8}$$

$$M_{2\max} = 0.0282 S_a\left(T_2\right)\frac{W_{trib}}{g}h_w\left|\sin\frac{4.49h_j}{h_w} + \frac{0.976h_j}{h_w}\right| \tag{9}$$

$$M_{3\max} = 0.00384 S_a\left(T_3\right)\frac{W_{trib}}{g}h_w\left|\sin\frac{7.73h_j}{h_w} - \frac{0.991h_j}{h_w}\right| \tag{10}$$

The first mode contributions, M_{1max} and V_{1max}, are calculated using an overstrength factor, Ω. This overstrength factor is determined using the results of the design and analysis procedures (Section 3.1 and Section 2.2, respectively), as shown in Eqn. (11).

$$\Omega = \frac{M_{base}(\theta_{peak})}{M_{con}} \tag{11}$$

To calculate the higher mode contributions, an estimate of the higher mode periods (T_2, T_3) is required. T_2 and T_3 can be estimated by modal analysis of a fixed-base model of the controlled rocking CLT wall, even though the base rotational restraint is reduced from the fixed-base condition as the wall uplifts [Kovacs 2016; Wiebe and Christopoulos 2015]. In this study, modal analysis of the numerical model is used to determine T_2 and T_3 for design.

Next, the individual modal responses (i=1, 2, 3) are combined using Eqn. (12), presented by Wiebe and Christopoulos [2015b; c]. In this equation, r is the $M_{i,max}$ or $V_{i,max}$ response, which is always positive for i=1, and r_{total} represents the peak total response at height, h_j.

$$r_{total} = r_1 + \sqrt{r_2^2 + r_3^2} \tag{12}$$

Finally, the higher mode response estimates are compared to the controlled rocking CLT wall shear and bending moment capacities. The bending moment and shear capacities can be estimated as $M_{cap}=f_{b,eff}\cdot S$, and $V_{cap}=A_v\cdot f_{v,eff}$, respectively, where S is the section modulus, A_v is the shear area of the gross wall cross section, and $f_{b,eff}$ and $f_{v,eff}$ are the effective bending and shear strength of the timber panel [Blass and Fellmoser 2004]. If the higher mode responses exceed the respective capacities, then Ganey [2015] and Sarti [2015] suggested that multiple rocking sections [Wiebe and Christopoulos 2015b] could be used to mitigate the higher mode demands.

4. Prototype Designs

Using the procedure described above, three-, six-, and nine-storey controlled rocking CLT walls were designed for the seismic hazard of Montreal, Canada with a 2% probability of exceedance in 50 years. The three- and six-storey designs have the same dimensions, 54 m x 54 m (2,916 m^2), chosen because the maximum permitted building area for a six-storey building in Ontario is 3,000 square metres [Jeske and Esposito 2015]. The nine-storey design has a smaller footprint of 24 m x 24 m (576 m^2). This dimension is chosen to reflect that the allowable building area typically decreases with additional stories of a timber building [Jeske and Esposito 2015]. The storey height for all three prototypes is a nominal dimension of 3.3 metres. All three buildings were designed according to the Canadian building code [NRCC 2010] with 2.3 kPa dead load on the floors, and both 3 kPa dead load and 2.4 kPa snow load on the roof.

In all three designs, the CLT panel is 315 mm thick (i.e. "314-9L" [Nordic Structures 2015]), and the PT elements are 26 mm diameter bars [DSI 2015]. The 314-9L panel has double longitudinal layers on the outside faces of the panel, increasing compression resistance in the rocking toe and under the PT anchorage. Moreover, the central layer of the 314-9L is thick enough to allow for the 26 mm diameter PT element by including a channel in only one layer. Table 2 summarises the designs, and sample layouts are shown in Figure 5.

Table 2 - Summary of three prototype designs

	Three-storey	Six-storey	Nine-storey
Building Dimensions	54 m x 54 m x 9.9 m (3.3 m per storey)	54 m x 54 m x 19.8 m (3.3 m per storey)	24 m x 24 m x 29.7 m (3.3 m per storey)
No. of Walls	16	12	8

Wall length (m)	2.44	4.88	4.88
R	18	19	4
T_n (s)	0.74	1.04	1.09
M_{con} (kN·m) [1]	1,891 kN·m (seismic) 1,050 kN·m (wind)	5,350 kN·m (seismic) 5,170 kN·m (wind)	11,000 kN·m (seismic) 10,600 kN·m (wind)
θ_{peak} (% h_w)	2.3%	1.4%	0.5%
$T_{PT,init}$ per bar [2]	39 kN	32 kN	222 kN
PT bar location	600 mm from each wall end	1220 mm from each wall end	1220 mm from each wall end
[1] Design force for the whole building; single wall designed for M_{con}/number of walls [2] PT elements and configurations within the wall are identified below			

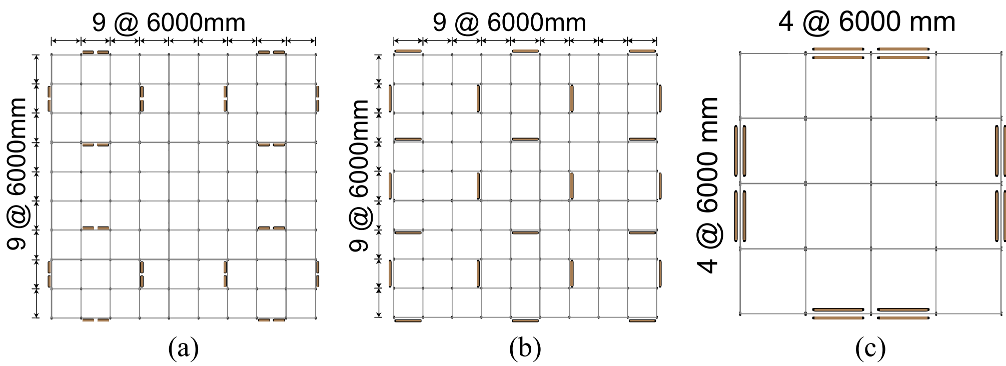

Figure 5 - Layouts of (a) three-, (b) six-, and (c) nine-storey designs

The prototypes were designed to minimise the seismic demand at the 2% in 50-year hazard level (MCE), while still limiting θ_{peak} to the 2.5% limit in the Canadian building code [NRCC 2010]. Moreover, *R* is limited to 19.0 and 4.0 in the six- and nine-storey designs, respectively, so as not to unnecessarily reduce the seismic demand below the wind demand. In designing to minimise seismic demand in the three-storey building, 2.44 m panels are specified to achieve a lower in-plane stiffness compared to the 4.88 m panels in the six- and nine-storey designs. With this panel dimension, the wall's relatively low in-plane elastic stiffness results in a relatively large elastic drift, and consequently a large estimated θ_{peak}. Therefore, the three-storey structure was designed using R = 18 in order to satisfy the limit on θ_{peak} of 2.5%.

Capacity design was considered following the method described in Section 3.2. The in-plane shear and bending strength values of 1.5 GPa and 19 GPa, respectively, were calculated using composite theory [Blass and Fellmoser 2004] with timber properties from Nordic Structures [2015]. The predicted demands were all less than half the estimated bending moment capacities (5,900 kN·m for the 2.44 m panel and 23,700 kN·m for the 4.88 m panel) and shear capacities (960 kN for the 2.44 m panel and 1,920 kN for the 4.88 m panel) for each wall. Therefore, capacity design did not govern the prototype designs.

5. Numerical Modelling

5.1 Model Construction

Figure 6 (a) shows a schematic of the controlled rocking CLT wall numerical model that was constructed in OpenSees [Mazzoni et al. 2006]. The model relies on the Winkler Spring Analogy (see Section 2.2) to capture the stresses in the controlled rocking CLT wall base. The Winkler springs, representing sub-elements of the base connection, are defined by zero-length elements with an elastic perfectly plastic gap material (Figure 6 (b)). This material does not have any stiffness in tension, but its axial compression stiffness is defined by the timber modulus of elasticity, the subarea of the base that the spring represents, and an effective length defined by Eqn. (1) at θ_{roof}=2%. Furthermore, the yield stress reflects the CLT crushing stress, defined by the species of timber in the CLT panel [Nordic Structures 2015].

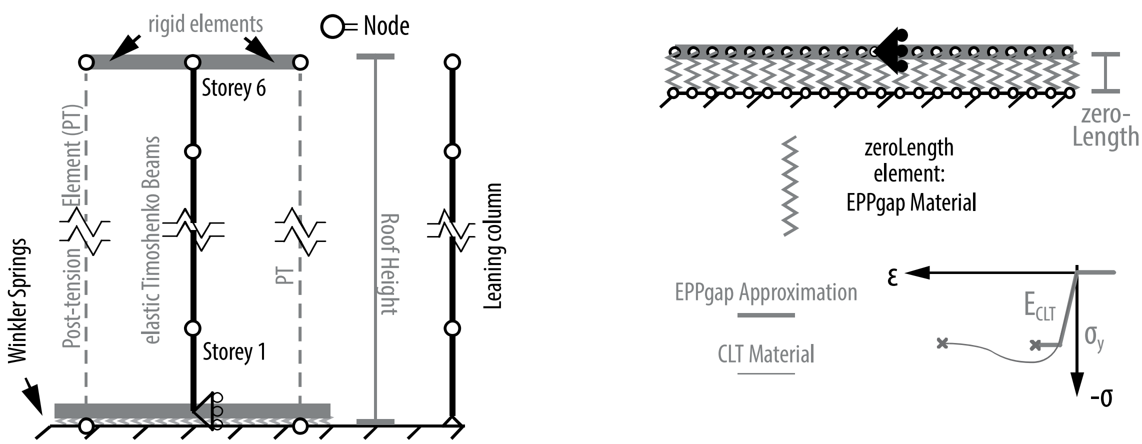

Figure 6 - (a) OpenSees numerical model; (b) Base connection (Winkler Springs), including the material model

The primary wall elements are represented in OpenSees by elastic Timoshenko beam elements, which capture both shear and bending deformations; the properties of the beam are included in Table 1. PT elements are represented by corotational truss elements with the Steel02 material model, using an initial stress that is calibrated to achieve $T_{PT,init}$ after the wall shortens under the initial compression. A spring is located at the bottom of the PT elements to prevent the PT from taking any compression. Rigid elements are modelled at the top and bottom of the wall panel to connect its centreline with the top of the PT elements, and the Winkler Springs at the base, as seen in Figure 6 (a).

A leaning column represents the gravity system associated with the controlled rocking CLT wall, capturing P-Delta effects in the model. Also, a tangent-stiffness Rayleigh damping model is applied to the numerical model, with 5% damping in the first and third modes. A value of 3% damping was determined from area-based viscous damping studies of post-tensioned specimens without supplemental energy dissipation [Marriott 2009; Sarti 2015], but the increase to 5% is intended to account for additional damping from non-structural elements in the building. The sensitivity of the results to the inherent damping assumption is discussed by Kovacs [2016].

For the purposes of these analyses, collapse was defined as an interstorey drift of 10% or more. To model excessive crushing, the MinMax material object in OpenSees is used to remove Winkler springs from the model when their strain exceeds two times the yield strain in compression. This conservative modelling assumption was made because Newcombe's [2011] empirical Winkler spring relationship is only calibrated up to twice the yield strain, even though Ganey [2015] showed that CLT could withstand larger strain demands before losing its compression capacity. Also, to model failure of the PT elements, they are removed if their strain exceeds 2%, corresponding with an ultimate PT stress of 1,030 MPa, to model crushing of the timber under the PT anchorage. The PT bars are capable of up to 9% strain [DSI 2015], so completely removing the PT element at only 2% strain is also considered to be conservative for this collapse fragility investigation.

Each baseline model is also associated with a lower-bound variation. In the lower-bound model, the bending stiffness, initial PT force, and shear stiffness are reduced by 30%, 25%, and 36%, respectively, to account for material property variability. Furthermore, in the lower-bound model, the Winkler springs within 200 mm of the rocking toe have a compression stiffness that is reduced by 40% to account for rocking toe damage, and the PT material properties are modified to capture timber crushing under the anchorage. These modifications were calibrated to bound the experimental results of Sarti [2015], as discussed by Kovacs [2016].

6. Ground Motion Selection & Scaling

The analyses were conducted using a suite of forty-four ground motions (eleven each of magnitude six and magnitude seven, from near and far sources) chosen from a set developed by Atkinson [2009] to represent Eastern North American seismic hazards. The median of the suite is scaled to the 5%-damped uniform hazard spectrum for Montreal, Canada [NRCC 2010] at periods of 0.74 s, 1.04 s, and 1.09 s for the three-, six-, and nine-storey designs, respectively, resulting in ground motion suites with scaling factors of 1.430, 1.315, and 1.450, respectively. Figure 7 shows the spectra scaled for the three-storey design, and the scaled suites are similar for all three structures. Note that the design level in the Canadian building code is 2% in 50 years, referred to here as the Maximum Considered Earthquake (MCE). Further details about the ground motion selection and scaling are provided by Kovacs [2016].

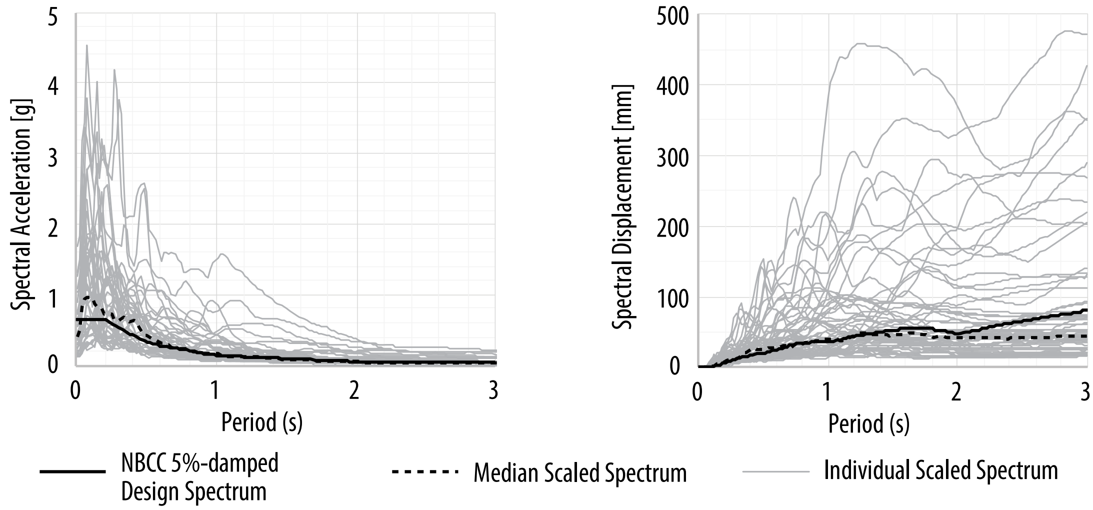

Figure 7 - Scaled response spectra for analysis of the three-storey design

7. Modelled Performance Under Maximum Considered Earthquake

Figure 8 shows response envelopes from the MCE-level suite for the baseline three-, six-, and nine-storey models. The lower-bound results were generally similar [Kovacs 2016]. The displacement results in Figure 8 show that the θ_{peak} estimates from the design procedure are significantly larger than the median θ_{peak} from NLTHA, especially for the three-storey building. This is because the ground motions used in this study generally underestimate the uniform hazard spectrum for periods longer than the initial periods of the design (see Figure 7), and this may underestimate the demand when the structure softens due to rocking. In addition, the C_R factors were calibrated for relatively low-frequency west coast records and systems with supplemental energy dissipation (i.e. energy dissipation ratio of $\beta \geq 20\%$), and were shown by Zhang [2015] to overestimate the median response for cases without energy dissipation (i.e. $\beta = 0$).

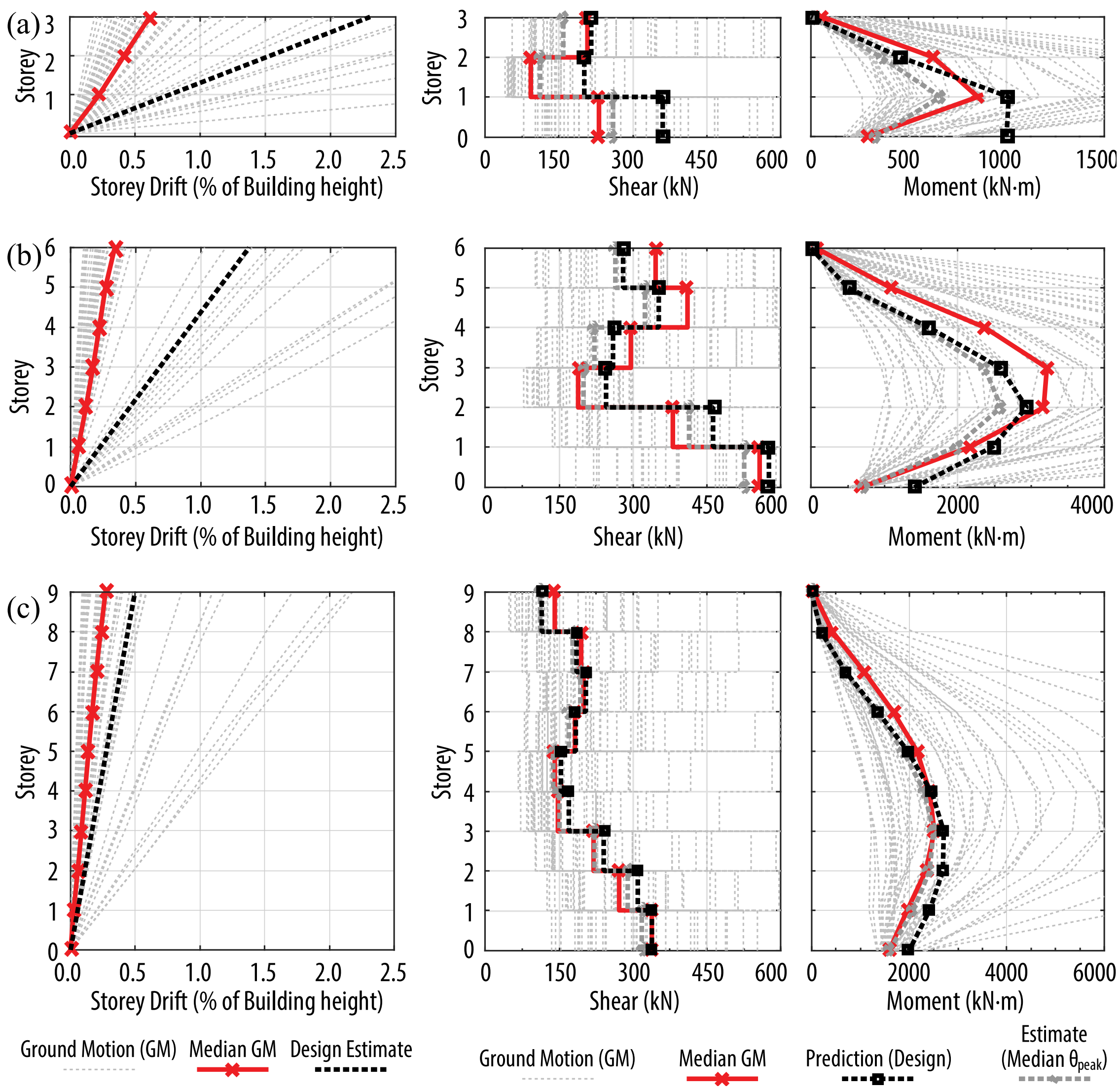

Figure 8 - Peak storey displacements, and shear and bending moment response envelopes in (a) three-, (b) six-, and (c) nine-storey controlled rocking CLT walls

The median peak shear and bending moment responses from NLTHA are shown in Figure 8, along with two dashed envelopes. One envelope is predicted using the θ_{peak} that was estimated during design, and the other is an estimate using the median θ_{peak} from NLTHA. The predicted envelope, based on the predicted θ_{peak}, overestimates the median shear and bending moment response at the base. However, the similarity improves with increasing prototype height: the base shear and bending moment overestimates are 50% and 200%, respectively, in the three-storey model, but only 0.3% and 10% in the nine-storey model. This prediction improves in the taller prototype because the θ_{peak} estimate only influences the first-mode contribution to the higher mode response estimate (Eqn. (5) and (8)), and the first-mode response has a decreasing influence on the force envelopes as the height increases. Despite the differences between the predictions and NLTHA results at the base, the peak overturning moment over the height is estimated to within 25% for the three-storey case, improving to within 2% in the nine-storey case, using the value of θ_{peak} that was estimated during design.

When the response envelopes are estimated using the actual median θ_{peak} from NLTHA instead of the predicted θ_{peak}, the results are generally closer to the median response at the base, with a maximum difference is less than 10%. Above the base, the estimated bending moment response envelope underestimates the peak median NLTHA bending moment by 23%, 24%, and 1%, in the three-, six-, and nine-storey prototypes. These results show that the overestimate of shear and bending moment from design are primarily because of the overestimate of θ_{peak}. However, regardless of how θ_{peak} is determined, the predicted shear and bending moment envelopes are more similar to the median NLTHA results as the height increases. This is likely because the cantilever beam analogy assumes uniformly distributed mass and stiffness, which is a more appropriate assumption for the taller prototype.

8. Incremental Dynamic Analysis

Incremental dynamic analysis is used to calculate the probability of collapse of the three prototypes at different earthquake intensities, as well as the probability of exceeding the shear or bending moment capacity of each wall. Incremental dynamic analysis results are presented using multiple stripes analysis [Jalayer 2003] in the following subsections. By counting the number of limit state occurrences at a limited number of intensity measures, multiple stripes analysis can efficiently estimate fragility parameters from the observed data [Baker 2015]. Although the multiple stripes analysis procedure is not sensitive to the selection of intensity measures, the maximum likelihood estimation of collapse fragility parameters becomes more accurate as the number of intensity measures increases [Baker 2015]. Therefore, the ground motion suites are scaled from 50% to 700% of the MCE at 50% increments.

8.1 Collapse Fragility Assessment

Each collapse fragility curve presented in Figure 9 is defined by a collapse margin ratio (θ) and record-to-record variability (β_{RTR}) parameter, as shown on each plot, determined from the maximum likelihood estimation procedure. Additionally, Table 3 summarises θ, and includes another variability parameter, β, for each of the three prototypes. The β values in Table 3 include not only the β_{RTR} value, but also additional terms for uncertainty in design requirements (β_{DR}), modelling (β_{MDL}), and in the test data (β_{TD}). These terms are combined using Eqn. (13), where β_{DR}, β_{MDL}, and β_{TD} are each 0.5, which is the most conservative value suggested by the FEMA P695 performance evaluation procedure [Applied Technology Council 2009]. This corresponds with the FEMA P695 qualitative rating of "poor", and is selected to account for relatively high uncertainties in the controlled rocking CLT wall. Further testing and more detailed design requirements are required to improve this rating by minimising uncertainty.

Table 3 - Fragility curve parameters and probability of collapse due to MCE event for baseline & lower-bound models

	Three-storey			Six-storey			Nine-storey		
	θ	**β**	**P[1](%)**	**θ**	**β**	**P[1](%)**	**θ**	**β**	**P[1](%)**
Baseline	5.21	1.4	11.7	7.51	1.5	9.6	9.64	1.7	9.2
Lower-bound	8.48	1.6	9.7	9.84	1.5	6.7	9.90	1.4	5.6

[1] Probability of collapse due to MCE-event

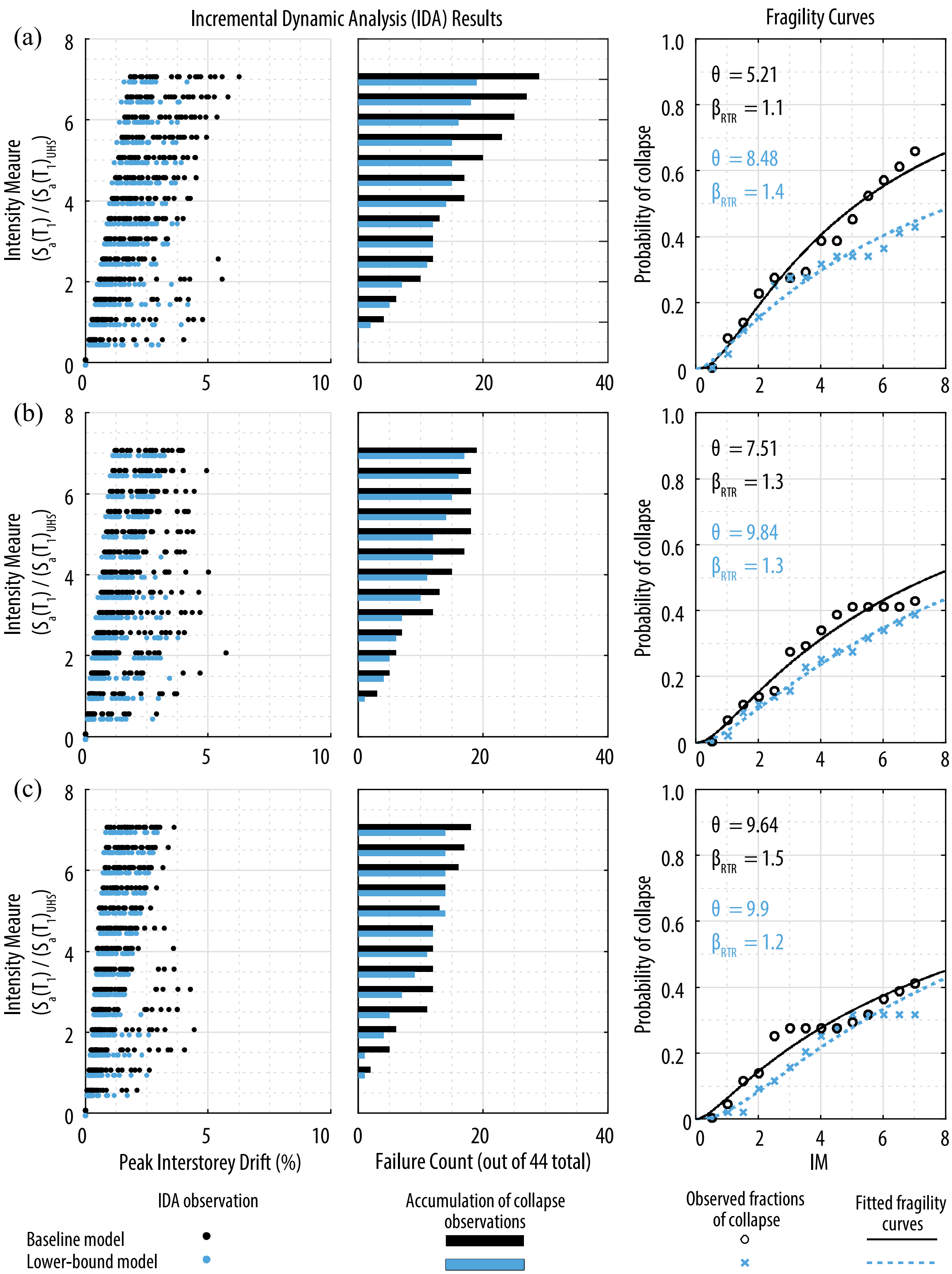

Figure 9 - Collapse IDA results for baseline and lower-bound models of (a) three-, (b) six-, and (c) nine-storey controlled rocking CLT walls

$$\beta = \sqrt{\beta_{RTR}{}^2 + \beta_{DR}{}^2 + \beta_{MDL}{}^2 + \beta_{TD}{}^2} \tag{13}$$

Table 3 also includes the probability of collapse at the MCE level, calculated from the fragility curve defined by θ and β. At the MCE level, the collapse probability is between 9.2% and 11.7% in the baseline three-, six-, and nine-storey models; 10% is the limit in the FEMA P695 performance evaluation procedure [Applied Technology Council 2009]. For all three buildings, failure generally occurred because the Winkler springs at the rocking toe reached their strain limit and were removed from the model. This led to an unzipping effect, in which the force associated with that spring shifted to the adjacent spring, quickly leading to its failure. This rocking toe failure occurred progressively until the model was considered to have collapsed at 10% drift, as demonstrated by Figure 10. This was considered a conservative way of modelling the timber response at large strains, recognizing that the complete loss of base connection compression capacity at large drifts is unlikely [Ganey 2015].

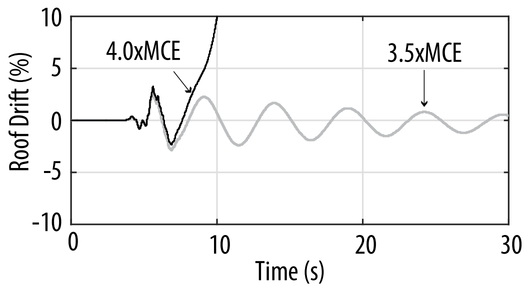

Figure 10 - Roof drift time-history demonstrating collapse in the baseline three-storey prototype, subjected to a magnitude six, near-source event

The lower-bound three-, six-, and nine-storey models demonstrate a lower probability of collapse due to an MCE-level event compared to the baseline model, as shown in Table 3. This is because the rocking toe material for the lower-bound model has a lower stiffness, which results in a larger yield strain for the rocking toe springs. This, in turn, allows a larger rocking motion to occur before the Winkler spring is removed from the model.

FEMA P695 also suggests a multiplier, called the spectral shape factor, to increase θ. The spectral shape factor accounts for differences between the spectral response of a rare seismic event and the shape of the design response spectrum [Applied Technology Council 2009], and it has the effect of reducing the calculated probability of collapse. Because no values of the spectral shape factor have been determined for the ground motions used in this study, the spectral shape factor is not applied here.

8.2 Bending Moment and Shear Fragility Assessment

The left sides of Figures 11 and 12 show the incremental dynamic analysis results for both the baseline and lower-bound three-, six-, and nine-storey models, considering the ratio of the maximum shear and bending moment demands over the height of the wall to their respective capacities. The middle plots show a cumulative histogram of the number of records in which the demand-capacity ratio exceeded one, for each intensity measure. The fragility curves on the right side (with parameters summarised in Table 4) show that there is a less than 4% chance of the shear or bending moment demand exceeding the capacity in the three-, six-, and nine-storey models at the MCE level. Note that exceedance indicates the possibility of a shear or bending failure in the timber panel, which could change the behaviour of the controlled rocking CLT wall, but it does not necessarily indicate collapse. The lowest probabilities of exceedance are in the lower-bound models because the reduced bending stiffness elongates the higher mode periods, reducing the spectral demands (see Figure 7).

Table 4 - Shear and bending moment demand-capacity curve parameters

		Three-storey			**Six-storey**			**Nine-storey**		
		θ	**β_{RTR}**	**P[1](%)**	**θ**	**β_{RTR}**	**P[1](%)**	**θ**	**β_{RTR}**	**P[1](%)**
Shear	**Baseline**	3.87	0.71	2.8	3.13	0.64	3.8	5.16	0.76	1.5
	Lower-bound	4.44	0.74	2.2	3.73	0.68	2.5	6.33	0.69	0.4
Bending Moment	**Baseline**	5.39	0.85	2.3	5.27	0.72	1.0	7.18	0.96	2.0
	Lower-bound	6.62	0.91	1.9	7.09	0.86	1.1	8.37	0.85	0.6

[1] Probability of exceedance due to MCE-event

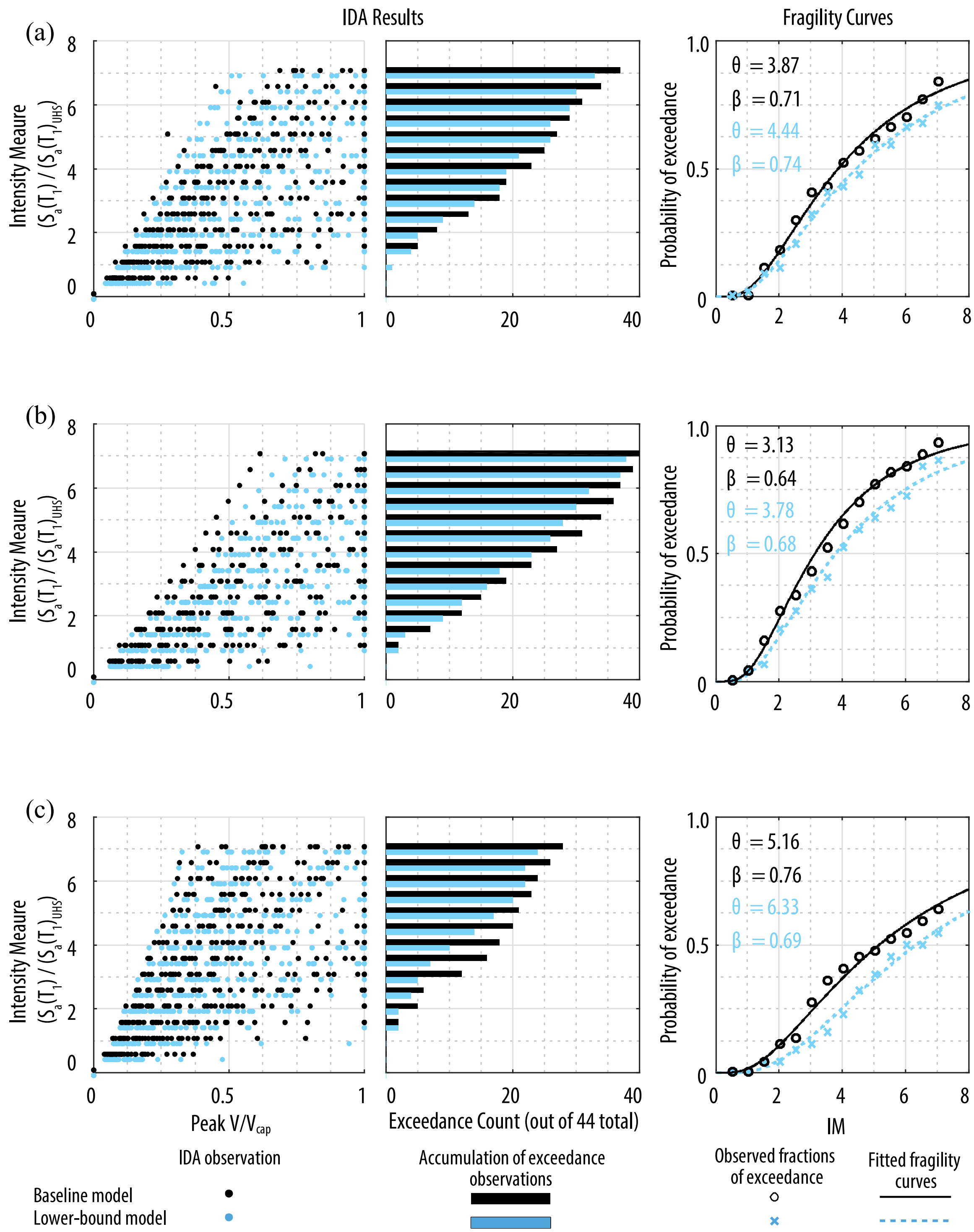

Figure 11 - Shear demand-capacity IDA results for baseline and lower-bound models of (a) three-, (b) six-, and (c) nine-storey controlled rocking CLT walls

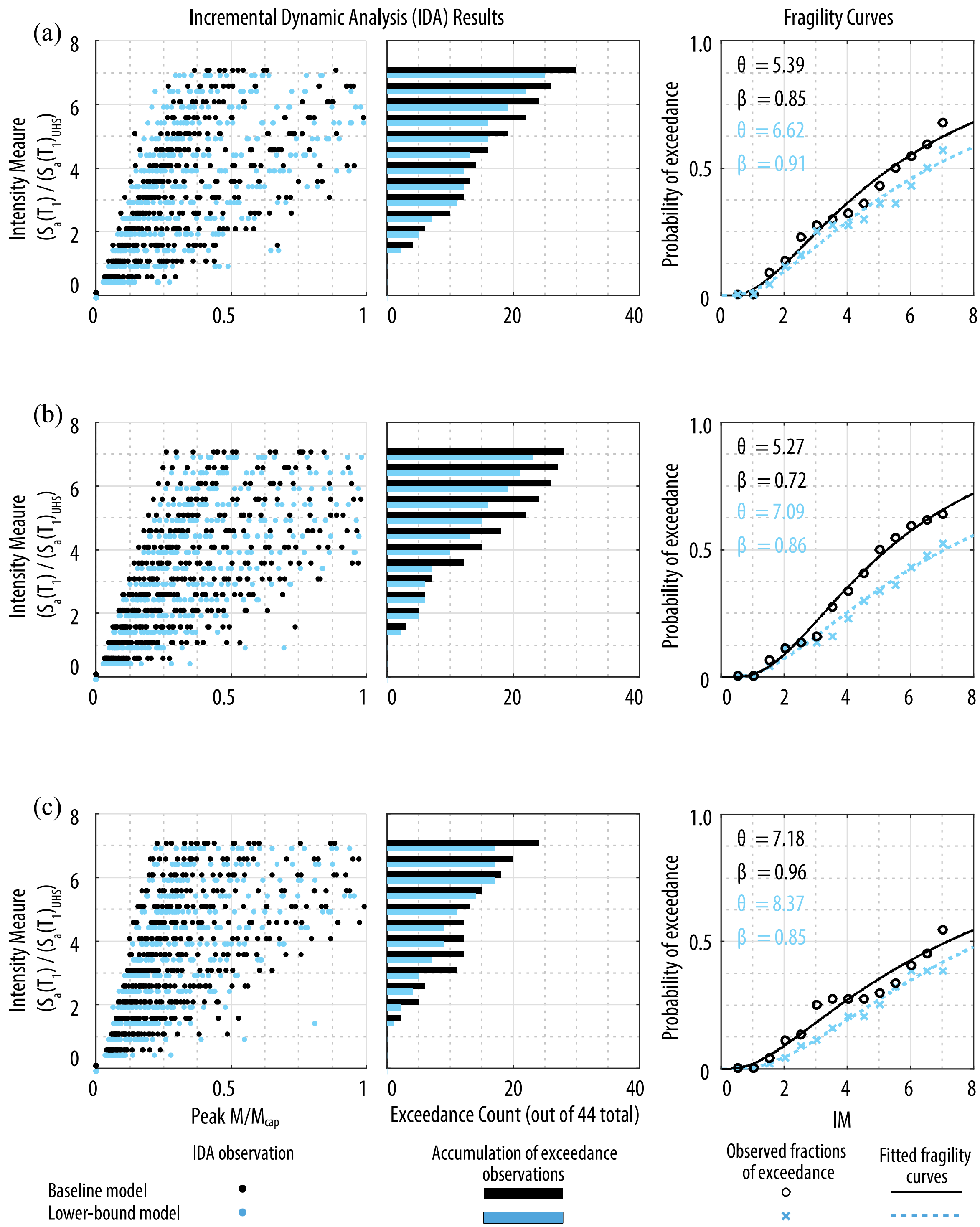

Figure 12 - Bending moment demand-capacity IDA results for baseline and lower-bound models of (a) three-, (b) six-, and (c) nine-storey controlled rocking CLT walls

8.3 Comparisons of Limit States

Figure 13 compares all three fragility curves, defined by their respective θ (median) and β_{RTR} (record-to-record variability) parameters, for both the baseline and lower-bound models of the three-, six-, and nine-storey designs. Both the median and the variability are lower for the shear and bending moment fragility curves than for the collapse fragility curves. The lower median increases the probability of occurrence at the MCE level, but the lower variability results in a steeper fragility curve. The combined effect is that the probability of shear and bending moment capacity exceedance at the MCE level is lower than the probability of collapse. In addition, it is less likely that the bending moment capacity is exceeded compared to the shear capacity.

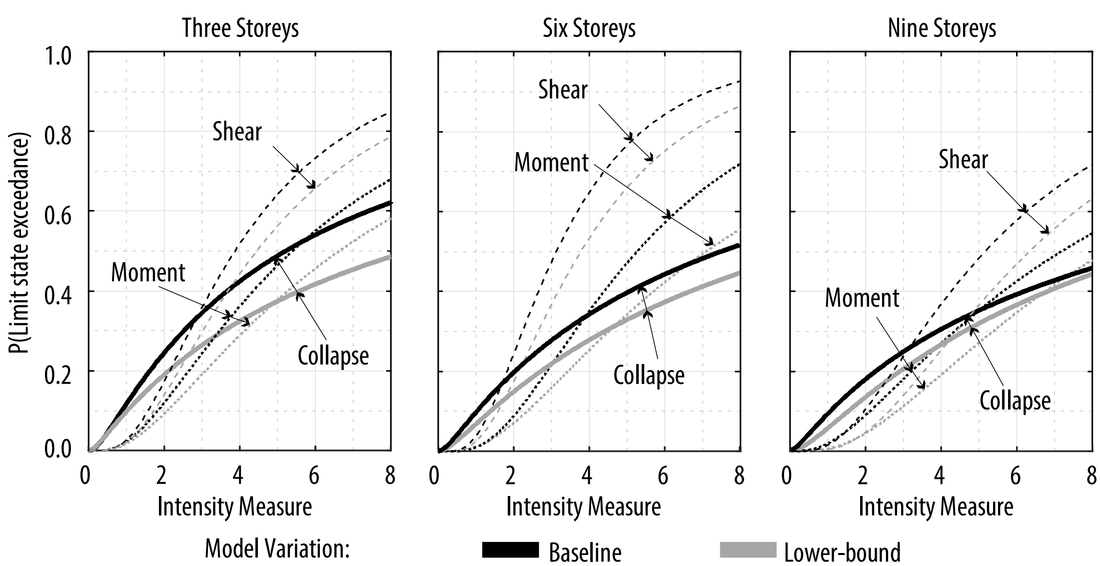

Figure 13 - Controlled rocking CLT wall fragility curves including collapse, and shear and bending moment capacity exceedance

At very large intensity measures, the shear and bending moment fragility curves exceed the collapse fragility curves. Although capacity exceedance is likely to damage the controlled rocking CLT wall, it does not necessarily mean collapse of the model. This means that the shear and bending moment limit states could affect the collapse fragility curves at large intensities, because the performance of the models would reduce if the shears or bending moments became excessive. However, at lower intensity measures, collapse due to base joint over-rotation is expected to occur before the shear or bending moment capacity is exceeded. Therefore, modelling the performance of the walls after exceeding the shear and bending moment capacity is expected to have little effect on the probability of collapse at relatively low intensities, including at the MCE level.

9. Conclusions

This paper presents a post-tensioned controlled rocking heavy timber wall made of cross-laminated timber (CLT) for regions of moderate seismicity, in which supplemental energy dissipation elements are omitted. A force-based design procedure is outlined in which the force-reduction factor is selected to minimise the seismic design forces, while still controlling the peak displacement to within building code limits and avoiding uplift under wind loads. The design methodology also includes a higher mode estimation procedure, adapted from controlled rocking steel braced frame research, for capacity design of the wall above the base. The design procedures are used to design three-, six-, and nine-storey prototype controlled rocking CLT walls for Montreal, Canada, using force-reduction factors of 18, 19, and 4, respectively. The three-storey design is controlled by the estimated peak drift limit of 2.5%, while the six- and nine-storey prototypes are designed for a seismic demand that is within 10% of the wind demand.

The controlled rocking CLT walls are numerically modelled in OpenSees, including a lower-bound variation based on modifications to the numerical model, to match experimental data by others. The models are subjected to nonlinear time-history analyses (NLTHA) to investigate the peak drift and higher mode response of the controlled rocking CLT wall at the MCE level. The peak roof drift estimated in design is larger than the median NLTHA results, because of the higher frequency content of the ground motions in this paper relative to those that are used to calibrate the displacement estimate. However, the estimated peak shears and bending moments capture the median NLTHA results to within 15% in all cases.

The models are also subjected to an incremental dynamic analysis procedure, which demonstrates that the baseline and lower-bound models have a 9.2%-11.7% and 5.2%-9.7% probability of collapse at the MCE level, respectively. Only the three-storey model exceeds the FEMA P695 suggested collapse probability limit of 10%. In this case, the model collapses soon after the range of calibration of the springs representing CLT crushing, even though this would not necessarily lead to collapse. Moreover, the design and modelling uncertainty are estimated conservatively when calculating the collapse probabilities, and no spectral shape factor is applied. Therefore, these collapse probability estimates are expected to be conservative. Moreover, all models have less than 5% probability of exceeding the shear or bending moment capacities at the MCE level.

Although the results suggest that the probability of collapse is close to the FEMA P695 collapse limits, the CLT properties at the base are modelled as bilinear, and the CLT elements are removed when they reach twice the yield strain. To account for modelling uncertainty, a lower-bound numerical model is also considered in this study, in which the timber strength and stiffness are reduced and the post-tensioning properties are modified to model some timber crushing under the anchorage. The collapse performance of this model is similar to the baseline model, but slightly better because of the larger displacement capacity. However, additional experimental testing of controlled rocking CLT panels is required to develop more accurate and reliable base connection models. Moreover, experimental validation of the concept proposed in this paper is needed before it could be applied in practice.

Furthermore, the numerical model does not capture the shear or bending moment failure response of the controlled rocking CLT wall. These limit states are not likely to occur at the MCE level, and they are not expected to cause immediate collapse. However, they are shown to be more likely to occur than collapse due to excessive drift at larger intensities. Therefore, the bending moment and shear failure response of larger scale specimens should be investigated and incorporated in the numerical model for future collapse assessments.

References

Applied Technology Council. [2009] *Quantification of Building Seismic Performance Factors*, *FEMA Report P695*, Washington, D.C.

Atkinson, G. M. [2009] "Earthquake time histories compatible with the 2005 National building code of Canada uniform hazard spectrum," *Canadian Journal of Civil Engineering*, Vol. 36, No.6, pp. 991–1000.

Baker, J. W. [2015] "Efficient analytical fragility function fitting using dynamic structural analysis," *Earthquake Spectra*, Vol. 31, No.1, pp. 579–599.

Blaikie, P., Cannon, T., Davis, I., and Wisner, B. [2003] *At Risk: Natural Hazards, People's Vulnerability and Disasters*, Routledge, Oxon, United Kingdon.

Blass, H. J., and Fellmoser, D. P. [2004] "Design of Solid Wood Panels With Cross Layers."

Davies, M., and Fragiacomo, M. [2011] "Long-Term Behavior of Prestressed LVL Members. I: Experimental Tests," *Journal of Structural Engineering*, Vol. 137, No.12, pp. 1553–1561.

DSI. [2015] "DYWIDAG Post-Tensioning System using Bars," DYWIDAG Systems International.

Fischer III, H. W., Scharnberger, C. K., and Geiger, C. J. [1996] "Reducing seismic vulnerability in low to moderate risk areas," *Disaster Prevention and Management*, Vol. 5, No.4, p. 5.

Flaig, M., and Blass, H. J. [2013] "Shear Strength and Shear Stiffness of CLT-Beams Loaded In Plane," *CIB-W18/46-12-3*, Vancouver, B.C.

Ganey, R. S. [2015] "Seismic Design and Testing of Rocking Cross Laminated Timber Walls," *Master of Science*, University of Washington.

Iqbal, A., Pampanin, S., Fragiacomo, M., Palermo, A., and Buchanan, A. H. [2012] "Seismic Response of Post-Tensioned LVL Walls Coupled With Plywood Sheets," *World Conference on Timber Engineering*, pp. 5–10.

Iqbal, A., Pampanin, S., Palermo, A., and Buchanan, A. H. [2015] "Performance and Design of LVL Walls Coupled with UFP Dissipaters," *Journal of Earthquake Engineering*, no, Vol. 19, No.3, pp. 383–409.

Jalayer, F. [2003] "Direct probabilistic seismic analysis: implementing non-linear dynamic assessments," *Department of Civil and Environmental Engineering*, *Doctor of Philosophy*, Stanford University.

Jeske, J., and Esposito, D. [2015] *2015 Reference Guide: Mid-Rise Wood Construction in the Ontario Building Code*, North Bay, Ontario.

KLH UK. [2015] "Technical," <http://www.klhuk.com/product-/technical.aspx> (Sep. 25, 2015).

Kovacs, M. [2016] "Seismic Design of Controlled Rocking Heavy Timber in a Low-to-Moderate Seismic Context," McMaster University.

Marriott, D. [2009] "The Development of High-Performance Post-Tensioned Rocking Systems for the Seismic Design of Structures," *Doctor of Philosophy*, University of Canterbury.

Mazzoni, S., McKenna, F., Scott, M. H., and Fenves, G. L. [2006] *OpenSees Command Language Manual*, Pacific Earthquake Engineering Research (PEER) Center, Berkeley, California.

Morris, H., Wang, M., and Zhu, X. [2012] "Deformations and Loads in an LVL Building with 3-Storey Post-Tensioned Shear Walls," *World Conference on Timber Engineering*, Auckland, New Zealand.

Moses, D., and Gagnon, S. [2010] "A New Generation of Solid Wood Panels," *Wood Design & Building*, pp. 40–44.

Natural Resources Canada. [2013] "The Potential of Cross Laminated Timber in North American Construction," *Canadian Forest Service Spotlight*, <http://publications.gc.ca/collections/collection_2013/rncan-nrcan/Fo12-44-2013-1-eng.pdf> (Apr. 8, 2015).

Newcombe, M. P. [2011] "Seismic Design of Post-Tensioned Timber Frame and Wall Buildings," *Doctor of Philosophy*, University of Canterbury.

Newcombe, M. P. [2015] "The Connection Response of Rocking Timber Walls," *SESOC Journal*, Vol. 28, No.1, pp. 46–53.

Nordic Structures. [2015] "Nordic X-LAM Cross-Laminated Timber (CLT)," <http://nordic.ca/en/products/nordic-x-lam-cross-laminated-timber-clt> (Sep. 25, 2015).

NRCC. [2010] *National Building Code of Canada - Chapter 4*, Canadian Commission on Building and Fire Codes.

Palermo, A., Pampanin, S., Buchanan, A. H., and Newcombe, M. P. [2005] "Seismic design of multi-storey buildings using laminated veneer lumber (LVL)," *New Zealand Society of Earthquake Engineering Conference*, Wairakei, New Zealand.

Pei, S., Rammer, D., Popovski, M., Williamson, T., Line, P., and Lindt, J. W. Van De. [2016] "An Overview of CLT Research and Implementation in North America," *Wcte2016*, No.September.

Sarti, F. [2015] "Seismic Design of Low-Damage Post-Tensioned Timber Wall Systems," *Doctor of Philosophy*, University of Canterbury.

Sarti, F., Palermo, A., and Pampanin, S. [2015] "Quasi-Static Cyclic Testing of Two-Thirds Scale Unbonded Posttensioned Rocking Dissipative Timber Walls," *Journal of Structural Engineering*, No.2008, p. E4015005.

Structural Timber Association. [2014] *Engineered wood products and an introduction to timber structural systems*, Alloa, UK.

Tsinker, G. P. [1997] *Handbook of Port and Harbor Engineering*, *Handbook of Port and Harbor Engineering: Geotechnical and Structural Aspects*, Springer US, Boston, MA, MA.

Wiebe, L., and Christopoulos, C. [2015a] "Performance-Based Seismic Design of Controlled Rocking Steel Braced Frames. I: Methodological Framework and Design of Base Rocking Joint," *Journal of Structural Engineering*, Vol. 141, No.9, p. 04014226.

Wiebe, L., and Christopoulos, C. [2015b] "Performance-Based Seismic Design of Controlled Rocking Steel Braced Frames. II: Design of Capacity-Protected Elements," *Journal of Structural Engineering*, Vol. 141, No.9, p. 04014227.

Wiebe, L., and Christopoulos, C. [2015c] "A cantilever beam analogy for quantifying higher mode effects in multistorey buildings," *Earthquake Engineering & Structural Dynamics*, Vol. 44, No.11, pp. 1697–1716.

Yeoh, D., Carradine, D., Palermo, A., Shrestha, R., and Morris, H. [2012] *Long-Term Performance of Post-Tensioned LVL Frames and Walls*, Canterbury, NZ.

Zhang, C. [2015] "Seismic Displacement Demands On Self-Centering Single-Degree-of-Freedom Systems," *Master of Applied Science*, McMaster University.